Contemporary Mathematics
https://ojs.wiserpub.com/index.php/CM/

Research Article

Theoretical and Numerical Simulation of a Discrete Fractional Order HIV Model with Latency

F. Gassem[1], Mohammed Almalahi[2,3], Ria Egami[4], Khaled Aldwoah[5], Abdelaziz Elsayed[6], Ashraf A. Qurtam[7]

[1]Department of Mathematics, College of Science, University of Hail, Hail, 55473, Saudi Arabia
[2]Department of Mathematics, College of Computer and Information Technology, Al-Razi University, Sana'a, 72738, Yemen
[3]Department of Mathematics, Faculty of Engineering and Information Technology, Al-Saeeda University, Sana'a, Yemen
[4]Department of Mathematics, College of Sciences in Sulail, Prince Sattam Bin Abdulaziz University, Saudi Arabia
[5]Department of Mathematics, Faculty of Science, Islamic University of Madinah, Madinah, 42351, Saudi Arabia
[6]Biology Department, Faculty of Science, Islamic University of Madinah, Madinah, Saudi Arabia
[7]Biology Department, College of Science, Imam Mohammad Ibn Saud Islamic University (IMSIU), Riyadh, 11432, Saudi Arabia
E-mail: aldwoah@iu.edu.sa

Received: 4 October 2025; **Revised:** 15 October 2025; **Accepted:** 28 October 2025

Abstract: This paper presents a novel discrete fractional-order mathematical model to describe the dynamics of Human Immunodeficiency Virus (HIV) infection, incorporating the critical role of latent reservoirs in $CD4^+$ T-cells. The model captures interactions among healthy T-cells, actively infected cells, latently infected cells, and free virus particles. By employing the Caputo fractional difference operator, the model accounts for memory effects and hereditary properties inherent in biological systems, which are often overlooked in traditional integer-order models. We establish the existence, uniqueness, boundedness, and non-negativity of solutions using Banach's fixed-point theorem and other analytical techniques. The basic reproduction number (R_0) is derived, and local stability conditions for both disease-free and endemic equilibria are determined via linearization. A sensitivity analysis identifies viral production and infection rates as the most influential parameters on R_0. Numerical simulations demonstrate how the fractional order (σ) modulates the infection dynamics, showing that stronger memory effects (lower σ) lead to a dampened acute viral burst but a higher chronic viral set point. The results underscore the utility of discrete fractional-order models in capturing key features of HIV progression, including latency and history-dependent behavior.

Keywords: Human Immunodeficiency Virus (HIV) model, fractional calculus, latency, stability analysis, bifurcation, basic reproduction number, sensitivity analysis

MSC: 92D30, 39A11, 26A33, 39A28

1. Introduction

The Human Immunodeficiency Virus (HIV) remains a formidable global health challenge, primarily due to its targeted depletion of $CD4^+$ T-cells-a cornerstone of the adaptive immune system. This progressive degradation leads to Acquired Immunodeficiency Syndrome (AIDS), severely compromising the host's ability to fight infections and diseases

Copyright ©2025 Khaled Aldwoah, et al.
DOI: https://doi.org/10.37256/cm.6620258807
This is an open-access article distributed under a CC BY license
(Creative Commons Attribution 4.0 International License)
https://creativecommons.org/licenses/by/4.0/

[1, 2]. A complete understanding of the intricate dynamics of virus-host interactions is therefore paramount for developing effective therapeutic and preventive strategies [3].

Mathematical modeling has emerged as an indispensable tool for deciphering the complex pathogenesis of HIV [4]. By translating biological mechanisms into mathematical formalism, these models provide critical insights into viral replication, immune cell dynamics, and the efficacy of interventions [5, 6]. The foundational work of Perelson [6] established a core framework that has been extensively expanded upon [7–9]. However, a significant limitation of most traditional models based on integer-order calculus is their inherent assumption of a Markovian, or memoryless, system. This overlooks the profound historical dependencies and long-term memory that characterize biological systems [10], such as the cumulative damage to the immune system or the slow, latent dynamics of viral reservoirs. For a more comprehensive review of HIV models, we refer the readers to the following papers [11–13] and the references therein. To better reflect the multifaceted nature of the epidemic, the scope of HIV modeling has been significantly broadened beyond foundational deterministic systems. Researchers have developed sophisticated computational and numerical frameworks to explore a variety of critical real-world complexities. These advanced studies have investigated the dynamics of co-infection with other viruses like Hepatitis C, the demographic impact of specific population groups on disease transmission, the influence of time-delay strategies on infection dynamics, and the role of stochastic effects within two-sex population models [14–16].

Fractional calculus, which generalizes differentiation and integration to non-integer orders, provides a powerful mathematical framework to incorporate these memory and hereditary properties [17]. Fractional-order models have been shown to offer a more accurate representation of complex biological processes [18–20] and often provide a superior fit to empirical data compared to their integer-order counterparts [21–23]. This efficacy is evidenced by their successful application across a spectrum of virological studies, including models of hepatitis [24, 25], multi-strain epidemics [26], and within immunology [27]. In the specific context of HIV, this memory effect can be linked to several biological phenomena: the slow, time-dependent maturation and clonal expansion of the immune response; the delayed reactivation of virus from latent reservoirs, which is influenced by the entire history of cellular activation; and the cumulative, non-instantaneous damage to the lymph node architecture and T-cell regenerative capacity. The fractional order σ thus serves as an index of the strength of these history-dependent processes.

The landscape of fractional calculus encompasses a diverse range of operators, each possessing unique characteristics and applications [28–30]. While we employ the Caputo operator for its utility in handling initial value problems common in biology, we acknowledge other operators like Atangana-Baleanu (AB) or Caputo-Fabrizio (CF), whose non-singular kernels could model different memory behaviors. A comparative study of these operators for HIV dynamics is a valuable direction for future work.

Concurrently, there is a growing recognition of the utility of discrete-time models, as clinical data-such as viral load and T-cell counts-are inherently collected at discrete intervals. The field of discrete fractional calculus [31] has thus gained traction, bridging the gap between continuous fractional theory and discrete data analysis, with applications in population dynamics [32], epidemiology [33], and other fields [34–36]. The utility of fractional operators extends beyond dynamic modeling to advanced numerical methods, such as fractional finite difference schemes and non-polynomial spline methods [37–40], highlighting their flexibility. This work leverages this flexibility to create a discrete fractional framework for biological systems.

A critical biological feature that any realistic HIV model must address is the establishment of a latent reservoir, where infected cells enter a dormant state, providing a sanctuary for the virus and presenting a major barrier to a cure. While some prior studies have explored fractional-order HIV models [9] or discrete integer-order models [41, 42], the unique synthesis of a discrete-time framework, fractional-order operators for memory, and an explicit latency pathway remains a significant and under-explored gap in the literature.

This paper addresses this gap, which makes three key novel contributions:

• We develop a novel discrete fractional-order model for HIV that explicitly incorporates a pathway to cellular latency, a key driver of viral persistence.

• We provide a rigorous mathematical analysis of the model, establishing the existence, uniqueness, boundedness, and non-negativity of solutions. We derive the basic reproduction number (R_0) and conduct a comprehensive stability and bifurcation analysis.

• We perform a sensitivity analysis to identify key parameters and use numerical simulations to demonstrate how the fractional order σ (the memory index) modulates the transition from acute to chronic infection, offering new biological insights.

The remainder of this paper is structured as follows: the model is formulated in section 2. Section 3 is dedicated to analyzing its fundamental properties, including boundedness, non-negativity, and existence and uniqueness of solutions. Equilibrium analysis and the sensitivity of R_0 are presented in section 4. Stability and bifurcation results are discussed in section 5. Numerical simulations and a comprehensive discussion of the results are provided in section 6. Finally, the paper concludes with a summary of findings and future directions in section 7.

2. Model formulation

Our decision to develop a discrete fractional-order model is deliberate and motivated by several factors aimed at enhancing biological realism and clinical applicability. The model was formulated according to the following logical progression:

• **Foundation on a Discrete Framework:** We began with a well-established discrete-time model that describes the core dynamics between uninfected T-cells ($\mathbb{U}$), actively infected T-cells ($\mathbb{I}$), and free virus ($\mathbb{V}$). This discrete foundation is inherently aligned with the nature of clinical data collection.

• **Introduction of a Latency Pathway:** A critical aspect of HIV infection is the formation of a latent reservoir, where infected cells enter a dormant state, allowing the virus to persist for years. To capture this, we introduce the term $\delta\mathbb{I}$, which represents the rate at which actively infected cells transition into a non-productive, latently infected state. This key feature is essential for modeling a primary barrier to a cure.

• **Incorporating the Fractional-Order Operator:** Biological processes, particularly immune responses, exhibit memory effects. The current state of the immune system is influenced by its entire history of pathogen encounters. To capture this hereditary property, we generalize the discrete model by replacing the standard first-order difference with the Caputo fractional difference operator. The fractional order $\sigma \in (0,\ 1]$ acts as a memory index, modulating the system's dependence on its past states and allowing the model to account for the cumulative impact of the infection over time.

The novel discrete model describes long-term relationships. It is formulated using the fractional derivative, specifically the Caputo difference operator as defined in [31]. This model extends the classical HIV dynamics framework established by Perelson and colleagues [9, 41, 43]. Here, it is modified to include a transition pathway to latency ($\delta\mathbb{I}$). The model is given as follows:

$$\begin{cases} {}^{C}\Delta^{\sigma}\mathbb{U}(\mu) = \tau - p\mathbb{U}(\mu-1+\sigma) + \varsigma\mathbb{U}(\mu-1+\sigma)\left(1-\dfrac{\mathbb{U}(\mu-1+\sigma)}{\mathbb{U}_{\max}}\right) \\ \qquad\qquad - k\mathbb{V}(\mu-1+\sigma)\mathbb{U}(\mu-1+\sigma) + \delta\mathbb{I}(\mu-1+\sigma), \\ {}^{C}\Delta^{\sigma}\mathbb{I}(\mu) = k\mathbb{V}(\mu-1+\sigma)\mathbb{U}(\mu-1+\sigma) - (\beta+\delta)\mathbb{I}(\mu-1+\sigma), \\ {}^{C}\Delta^{\sigma}\mathbb{V}(\mu) = N\beta\mathbb{I}(\mu+\sigma-1) - \gamma\mathbb{V}(\mu-1+\sigma)\ , \end{cases} \tag{1}$$

where $\mu \in [0,\ b]_{\mathbb{N}_0}$, and ${}^{C}\Delta^{\sigma}$ is the Caputo difference operator with order σ. The schematic diagram of the HIV/CD4^{+} T-cell model is presented in Figure 1.

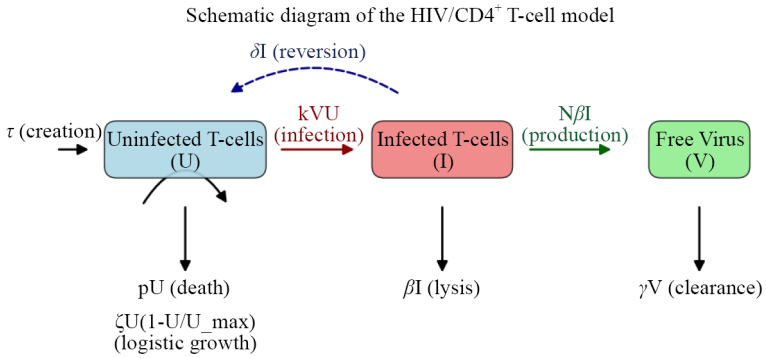


Figure 1. Schematic diagram of the HIV/CD4$^+$ T-cell model

The model variables are classified and defined in Table 1, while the parameters used in the model (1) are summarized in Table 2. The parameter values are derived from existing literature on HIV modeling to represent a biologically plausible scenario. No parameter estimation or calibration with a specific dataset was performed in this theoretical study.

Table 1. Model variables and their biological interpretations

Variable	Description and biological interpretation
$\mathbb{U}(\mu)$	Concentration of uninfected (healthy) CD4$^+$ T-cells, (cells/μL)
$\mathbb{I}(\mu)$	Concentration of actively infected CD4$^+$ T-cells, which produce virus, (cells/μL)
$\mathbb{V}(\mu)$	Concentration of free HIV virus particles, (virions/μL)

Table 2. Model parameters, definitions, and biological justifications. Values are chosen to represent a consensus from the HIV modeling literature [20, 41, 42] for a typical chronic infection

Parameter	Definition	Value	Biological justification
τ	Influx of new CD4$^+$ T-cells	2.9 cells/day	Represents constant production of new T-cells from the thymus.
p	Natural death rate of uninfected T-cells	0.01/day	Corresponds to the standard lifespan of a healthy T-cell (approx. 69 days).
ς	Logistic growth rate of T-cells	0.001/day	Models slow, density-dependent proliferation to replenish depleted T-cell populations.
U_{max}	Carrying capacity of T-cell population	1,500 cells	Reflects the upper limit of a healthy T-cell count (500-1,600 cells/μL).
k	Per capita infection rate	8.0×10^{-5}	Calibrated to ensure $R_0 > 1$, a necessary condition for establishing a persistent infection.
δ	Transition rate to latency	0.2/day	Represents the fraction of infected cells that enter a resting state, forming the latent reservoir.
β	Death rate of actively infected T-cells	0.16/day	High death rate ($\beta \gg p$) due to viral cytopathic effects and immune clearance.
N	Viral burst size per infected cell	1,000 virions/cell	Represents the large number of virions produced by a single infected cell over its lifespan.
γ	Clearance rate of free virus	3.4/day	Reflects the very short half-life of free virions in the blood (approx. 5 hours) due to rapid immune clearance.

2.1 *Assumptions and characteristics of the model*

The model is built upon the following assumptions and characteristics:

• Logistic Growth of $CD4^+$ T-cells: The model incorporates the logistic growth of uninfected $CD4^+$ T-cells, represented by the term $\varsigma\mathbb{U}\left(1-\frac{\mathbb{U}}{\mathbb{U}_{max}}\right)$. This term reflects density-dependent proliferation, where the growth rate decreases as the uninfected $CD4^+$ T-cell population ($\mathbb{U}$) approaches its carrying capacity ($\mathbb{U}_{max}$).

• Infection Dynamics: Infection occurs via a bilinear term $k\mathbb{V}\mathbb{U}$, where the infection rate depends on the interaction between the free virus and uninfected T-cells.

• Viral Production: Each actively infected $CD4^+$ T-cell contributes to viral load through the term $N\beta\mathbb{I}$.

• Transition to Latency: The term $\delta\mathbb{I}$ represents the rate at which actively infected cells transition to a latency state. This is a key biological process representing the formation of the latent HIV reservoir, which is the primary barrier to a cure. Our model captures this by removing cells from the actively infected pool.

• Simplification and Justification: The model does not incorporate the proliferation of infected $CD4^+$ T-cells and assumes that all parameters are positive constants. We assume that the death rate of infected cells is greater than or equal to the death rate of uninfected $CD4^+$ T-cells (i.e., $\beta \geq p$). This is biologically justified as actively infected cells face additional mortality from viral cytopathic effects and immune-mediated clearance [41]. The model is deterministic and intentionally ignores stochastic factors to focus on the average system behavior.

The Table 3 contrasts model features to highlight our contribution, and should not be seen as a performance benchmark. We aim to underscore the novelty of our model's architecture, which uniquely combines a discrete-time structure, fractional dynamics, and a latency pathway.

Table 3. Comparison of our model with key previous HIV models

Study	Model type	Framework	Key features included	Memory effects (σ)
Perelson [41]	ODE	Continuous	Core dynamics	No
Lichae et al. [9]	FDE	Continuous	Antiretroviral Therapy (ART), Latency	No
Jan et al. [43]	FDE	Continuous	HIV-Tumor interaction	No
This study	FDE	Discrete	Latency, Memory	Yes

Note: ODE = Ordinary Differential Equation, FDE = Functional Differential Equation.

3. Fundamental properties of the model

This section aims to analyze the fundamental properties of the HIV infection model (1) described by discrete fractional-order.

3.1 *Boundedness of the solutions*

To ensure the model is biologically plausible, we must prove that solutions remain non-negative and bounded. Non-negativity is essential as cell and virus populations cannot be negative. Boundedness ensures that populations do not grow infinitely, reflecting natural constraints within the host. Together, these properties confirm the model is well-posed.

Theorem 1 All solutions of the discrete fractional-order model (1) that originate in $\mathbb{R}^3_+$ are ultimately bounded. Specifically, there exists a bounded set $\Pi \subset \mathbb{R}^3_+$ that is a positively invariant and attracting region for the system, where

$$\Pi = \left\{(\mathbb{U},\, \mathbb{I},\, \mathbb{V}) \in \mathbb{R}^3_+;\, \mathbb{U}+\mathbb{I} \leq \frac{\tau}{p-\varsigma}+\varepsilon_1, \quad \mathbb{V} \leq \frac{N\beta\tau}{\gamma(p-\varsigma)}+\varepsilon_2\right\},$$

for any small positive constants ε_1 and ε_2.

Proof. The non-negativity of solutions for the discrete fractional-order system is established in Theorem 2. Here, we prove the boundedness of the solutions $\mathbb{U}(\mu)$, $\mathbb{I}(\mu)$, and $\mathbb{V}(\mu)$. Let us define a function for the total T-cell population, $M(\mu) = \mathbb{U}(\mu) + \mathbb{I}(\mu)$. We analyze its rate of change using the model (1), which describes the system's dynamics:

$$ {}^{C}\Delta^{\sigma} M(\mu) = {}^{C}\Delta^{\sigma} \mathbb{U}(\mu) + {}^{C}\Delta^{\sigma} \mathbb{I}(\mu). $$

Substituting the expressions from Equation (1), we have:

$$ {}^{C}\Delta^{\sigma} M(\mu) = \left[\tau - p\mathbb{U} + \varsigma \mathbb{U}\left(1 - \frac{\mathbb{U}}{\mathbb{U}_{\max}}\right) - k\mathbb{V}\mathbb{U} + \delta\mathbb{I} \right] + \left[k\mathbb{V}\mathbb{U} - (\beta + \delta)\mathbb{I} \right]. $$

By canceling the infection term $k\mathbb{V}\mathbb{U}$ and the latency-related term $\delta\mathbb{I}$, the expression simplifies to:

$$ {}^{C}\Delta^{\sigma} M(\mu) = \tau - p\mathbb{U} - \beta\mathbb{I} + \varsigma \mathbb{U}\left(1 - \frac{\mathbb{U}}{\mathbb{U}_{\max}}\right). $$

From our model assumptions, we have $\beta \geq p$, which is biologically justified as infected cells have a higher death rate. Let $d = \min(p,\ \beta)$. Since $p > 0$ and $\beta > 0$, we have $d > 0$. We can now establish an upper bound

$$ \begin{aligned} {}^{C}\Delta^{\sigma} M(\mu) &\leq \tau - p\mathbb{U} - p\mathbb{I} + \varsigma\mathbb{U} - \frac{\varsigma}{\mathbb{U}_{\max}}\mathbb{U}^2 \\ &\leq \tau - p(\mathbb{U} + \mathbb{I}) + \varsigma\mathbb{U} \\ &\leq \tau - pM + \varsigma M \quad (\text{since } \mathbb{U} \leq M) \\ &= \tau - (p - \varsigma)M. \end{aligned} $$

From the parameter values listed in Table 2, we have the natural death rate $p = 0.01$ and the logistic growth rate $\varsigma = 0.001$, which satisfies $p - \varsigma > 0$. This yields a standard linear differential inequality. This inequality implies that if $M(\mu) > \dfrac{\tau}{p - \varsigma}$, then ${}^{C}\Delta^{\sigma} M(\mu) < 0$. Therefore, the total T-cell population $M(\mu)$ cannot grow indefinitely and is ultimately bounded. By the theory of differential inequalities, we can conclude that the limit superior of $M(\mu)$ is bounded:

$$ \limsup_{\mu \to \infty} M(\mu) \leq \frac{\tau}{p - \varsigma}. $$

Let $M_1 = \dfrac{\tau}{p - \varsigma}$. This result guarantees that for any small $\varepsilon_1 > 0$, there exists a time μ_1 such that for all $\mu > \mu_1$, $\mathbb{U}(\mu) + \mathbb{I}(\mu) \leq M_1 + \varepsilon_1$. Consequently, the populations of uninfected T-cells $\mathbb{U}(\mu)$ and actively infected T-cells $\mathbb{I}(\mu)$ are also individually bounded. Next, we analyze the equation for the free virus population, $\mathbb{V}(\mu)$, from the continuous model:

$$^{C}\Delta^{\sigma}\mathbb{V}(\mu) = N\beta\mathbb{I} - \gamma\mathbb{V}.$$

From Step 1, we know that the infected cell population $\mathbb{I}(\mu)$ is bounded. For μ large enough ($\mu > \mu_1$), we have $\mathbb{I}(\mu) \leq M_1 + \varepsilon_1$. We can use this to establish an upper bound for $\mathbb{V}(\mu)$

$$^{C}\Delta^{\sigma}\mathbb{V}(\mu) \leq N\beta(M_1 + \varepsilon_1) - \gamma\mathbb{V}.$$

This is another linear differential inequality. If $\mathbb{V}(\mu) > \dfrac{N\beta(M_1+\varepsilon_1)}{\gamma}$, then $^{C}\Delta^{\sigma}\mathbb{V}(\mu) < 0$. This shows that the free virus population $\mathbb{V}(\mu)$ is also ultimately bounded. The limit superior of $\mathbb{V}(\mu)$ can be stated as:

$$\limsup_{\mu\to\infty} \mathbb{V}(\mu) \leq \frac{N\beta M_1}{\gamma}.$$

Thus, any trajectory starting in $\mathbb{R}^3_+$ will eventually enter and remain within the compact set Π. This completes the proof of boundedness for our proposed model. □

The boundedness of solutions is not merely a mathematical requirement but a critical biological constraint. It ensures that the populations of CD4$^+$ T-cells and free virus remain within physiologically plausible limits, reflecting the finite resources and spatial constraints within a host.

3.2 *Non-negativity of the solutions*

Theorem 2 For non-negative initial values, all solutions of model (1) are guaranteed to remain non-negative for all time.

Proof. Let $\mathbb{U}(0) \geq 0$, $\mathbb{I}(0) \geq 0$, and $\mathbb{V}(0) \geq 0$ be the initial conditions for system (1). By [31], we can write the equivalent summation form of the model (1), subject to the initial conditions $\mathbb{U}(0) \geq 0$, $\mathbb{I}(0) \geq 0$, and $\mathbb{V}(0) \geq 0$:

$$\begin{cases} \mathbb{U}(\mu) = \mathbb{U}(0) + \dfrac{1}{\Gamma(\sigma)} \displaystyle\sum_{s=1-\sigma}^{\mu-\sigma} (\mu - s - 1)^{\sigma-1} \mathbb{K}_1(\mu - 1 + \sigma, \mathbb{U}), \\ \mathbb{I}(\mu) = \mathbb{I}(0) + \dfrac{1}{\Gamma(\sigma)} \displaystyle\sum_{s=1-\sigma}^{\mu-\sigma} (\mu - s - 1)^{\sigma-1} \mathbb{K}_2(\mu - 1 + \sigma, \mathbb{I}), \\ \mathbb{V}(\mu) = \mathbb{V}(0) + \dfrac{1}{\Gamma(\sigma)} \displaystyle\sum_{s=1-\sigma}^{\mu-\sigma} (\mu - s - 1)^{\sigma-1} \mathbb{K}_3(\mu - 1 + \sigma, \mathbb{V}), \end{cases} \tag{2}$$

where

$$\begin{cases} \mathbb{K}_1(\mu-1+\sigma,\ \mathbb{U}) = \tau - p\mathbb{U}(\mu-1+\sigma) + \varsigma\mathbb{U}(\mu+\sigma-1)\left(1-\dfrac{\mathbb{U}(\mu-1+\sigma)}{\mathbb{U}_{\max}}\right) \\ \qquad\qquad - k\mathbb{V}(\mu-1+\sigma)\mathbb{U}(\mu+\sigma-1) + \delta\mathbb{I}(\mu-1+\sigma), \\ \mathbb{K}_2(\mu-1+\sigma,\ \mathbb{I}) = k\mathbb{V}(\mu+\sigma-1)\mathbb{U}(\mu-1+\sigma) - (\beta+\delta)\mathbb{I}(\mu-1+\sigma), \\ \mathbb{K}_3(\mu-1+\sigma,\ \mathbb{V}) = N\beta\mathbb{I}(\mu-1+\sigma) - \gamma\mathbb{V}(\mu-1+\sigma)\ . \end{cases} \tag{3}$$

Thus, all solutions of model (1) remain non-negative. □

This guarantee of non-negative solutions is essential for the model's biological validity, as negative concentrations of cells or viruses are physically impossible.

3.3 *Lipschitz property of the kernels* $\mathbb{K}_1,\ \mathbb{K}_2$ *and* $\mathbb{K}_3$

Theorem 3 Let $\mathbb{U},\ \mathbb{I},\ \mathbb{V},\ \widehat{\mathbb{U}},\ \widehat{\mathbb{I}},\ \widehat{\mathbb{V}}$ be continuous functions in $L^1[0,\ 1]$. Define positive constants $x_1,\ x_2$ and x_3 such that

$$\|\mathbb{U}\| = \max_{\mu\in\mathscr{J}} |\mathbb{U}(\mu)| < x_1,$$

$$\|\mathbb{I}\| = \max_{\mu\in\mathscr{J}} |\mathbb{I}(\mu)| < x_2,$$

$$\|\mathbb{V}\| = \max_{\mu\in\mathscr{J}} |\mathbb{V}(\mu)| < x_3.$$

Then, the kernels $\mathbb{K}_1,\ \mathbb{K}_2$ and $\mathbb{K}_3$ satisfy a Lipschitz property with Lipschitz constant $k = \max_{i=1}^{3}\{\mathscr{L}_{\mathbb{K}_i}\} > 0$, such that

$$\mathscr{L}_{\mathbb{K}_1} = \left((\varsigma-p) + \frac{\varsigma x_1}{\mathbb{U}_{\max}} + kx_2\right), \quad \mathscr{L}_{\mathbb{K}_2} = \beta, \quad \mathscr{L}_{\mathbb{K}_3} = \gamma.$$

Proof. For $\mathbb{K}_1(\mu-1+\sigma,\ \mathbb{U})$, let $\mathbb{U},\ \widehat{\mathbb{U}} \in L^1[0,\ 1]$. Then, we have

$$\left\|\mathbb{K}_1(\mu-1+\sigma,\ \mathbb{U}) - \mathbb{K}_1\left(\mu-1+\sigma,\ \widehat{\mathbb{U}}\right)\right\| \leq \left((\varsigma-p) + \frac{\varsigma x_1}{\mathbb{U}_{\max}} + kx_2\right)\left\|\mathbb{U}-\widehat{\mathbb{U}}\right\|.$$

Put $\mathscr{L}_{\mathbb{K}_1} = \left((\varsigma-p) + \dfrac{\varsigma x_1}{\mathbb{U}_{\max}} + kx_2\right) > 0$. Thus, we get

$$\left\|\mathbb{K}_1(\mu-1+\sigma,\ \mathbb{U}) - \mathbb{K}_1\left(\mu-1+\sigma,\ \widehat{\mathbb{U}}\right)\right\| \leq \mathscr{L}_{\mathbb{K}_1}\left\|\mathbb{U}-\widehat{\mathbb{U}}\right\|.$$

This leads to the following:

$$\left\|\mathbb{K}_2(\mu-1+\sigma,\,\mathbb{I})-\mathbb{K}_2\left(\mu-1+\sigma,\,\widehat{\mathbb{I}}\right)\right\|\leq\mathscr{L}_{\mathbb{K}_2}\left\|\mathbb{I}-\widehat{\mathbb{I}}\right\|,$$

and

$$\left\|\mathbb{K}_3(\mu-1+\sigma,\,\mathbb{V})-\mathbb{K}_2\left(\mu-1+\sigma,\,\widehat{\mathbb{V}}\right)\right\|\leq\mathscr{L}_{\mathbb{K}_3}\left\|\mathbb{V}-\widehat{\mathbb{V}}\right\|.$$

Let

$$k=\max_{i=1}^{3}\left\{\mathscr{L}_{\mathbb{K}_i}\right\}>0.$$

Thus, the kernels $\mathbb{K}_i,\ i=1,\ 2,\ 3$ are satisfied Lipschitz conditions with constant $k>0$. □

3.4 *Existence and uniqueness of the solution*

This subsection is devoted to proving the existence of solutions to the discrete fractional-order model (1). To this end, we employ a recursive sequence approach, leveraging the contraction mapping theorem to demonstrate the sequence's convergence to a unique solution. Now, we rewrite the model (1) in a compact operator form as follows:

$$\mathbf{X}(\mu)=\mathbf{X}_0+\frac{1}{\Gamma(\sigma)}\sum_{s=0}^{\mu-\sigma}(\mu-s-1)^{\sigma-1}\mathbf{F}(\mu-1+\sigma,\,\mathbf{X}(\mu-1+\sigma)),$$

where

$$\mathbf{X}(\mu)=\begin{pmatrix}\mathbb{U}(\mu)\\ \mathbb{I}(\mu)\\ \mathbb{V}(\mu)\end{pmatrix},\ \mathbf{X}_0=\begin{pmatrix}\mathbb{U}(0)\\ \mathbb{I}(0)\\ \mathbb{V}(0)\end{pmatrix},$$

and

$$\mathbf{F}(\mu-1+\sigma,\,\mathbf{X}(\mu-1+\sigma))=\begin{pmatrix}\mathbb{K}_1(\mu-1+\sigma,\,\mathbb{U})\\ \mathbb{K}_2(\mu-1+\sigma,\,\mathbb{I})\\ \mathbb{K}_3(\mu-1+\sigma,\,\mathbb{V})\end{pmatrix}.$$

Define the operator

$$\mathbf{H}(\mathbf{X}(\mu))=\mathbf{X}_0+\frac{1}{\Gamma(\sigma)}\sum_{s=0}^{\mu-\sigma}(\mu-s-1)^{\sigma-1}\mathbf{F}(\mu-1+\sigma,\,\mathbf{X}(\mu-1+\sigma)).\tag{4}$$

The recursive sequence of vector functions $\{\mathbf{X}_n(\mu)\},\ n=0,\ 1,\ 2,\ \ldots$ is defined by:

$$\mathbf{X}_{n+1}(\mu) = \mathbf{X}_0 + \frac{1}{\Gamma(\sigma)} \sum_{s=0}^{\mu-\sigma} (\mu - s - 1)^{\sigma-1} \mathbf{F}(\mu + \sigma - 1,\ \mathbf{X}_n(\mu - 1 + \sigma)).$$

The following theorem establishes the existence of a unique solution via a convergent iterative scheme.

Theorem 4 Assume that the components of $\mathbf{F}(\mu - 1 + \sigma,\ \mathbf{X}_n(\mu + \sigma - 1))$ are bounded and continuous for all $\mathbf{X}$ and $\mu \in [\sigma - 1,\ b + \sigma]_{\mathbb{N}_{\sigma-1}}$. Then, the model (1) possesses a solution provided that:

$$\frac{k\Gamma(b + \sigma + 1)}{\Gamma(\sigma + 1)\Gamma(b + 1)} < 1, \tag{5}$$

where k is the Lipschitz constant defined in Theorem 3.

Proof. Consider the operator (**H**) defined by (4). For all $\mathbf{X},\ \mathbf{Y} \in \mathbf{C}([0,\ T])$ and $\mu \in [\sigma - 1,\ b + \sigma]_{\mathbb{N}_{\sigma-1}}$, we have

$$\|\mathbf{H}(\mathbf{X}) - \mathbf{H}(\mathbf{Y})\| \leq \frac{1}{\Gamma(\sigma)} \sum_{s=0}^{\mu-\sigma} (\mu - s - 1)^{\sigma-1}$$

$$\|\mathbf{F}(\mu - 1 + \sigma,\ \mathbf{X}(\mu - 1 + \sigma)) - \mathbf{F}(\mu - 1 + \sigma,\ \mathbf{Y}(\mu - 1 + \sigma))\|.$$

By Theorem 3, $\mathbf{F}(\mu - 1 + \sigma,\ \mathbf{X}(\mu - 1 + \sigma))$ satisfies the Lipschitz condition $k = \max_{i=1}^{3} \{\mathscr{L}_{\mathbb{K}_i}\} > 0$. Then, we obtain that

$$\|\mathbf{H}(\mathbf{X}) - \mathbf{H}(\mathbf{Y})\| \leq \frac{k\|\mathbf{X} - \mathbf{Y}\|}{\Gamma(\sigma)} \sum_{s=0}^{\mu-\sigma} (\mu - s - 1)^{\sigma-1}.$$

The summation can be represented in terms of the Gamma function. Then, we get

$$\|\mathbf{H}(\mathbf{X}) - \mathbf{H}(\mathbf{Y})\| \leq \frac{k\Gamma(b + \sigma + 1)}{\Gamma(\sigma + 1)\Gamma(b + 1)} \|\mathbf{X} - \mathbf{Y}\|.$$

Then, according to the Banach fixed-point theorem, the operator $\mathbf{H}$ is a contraction. Therefore, the sequence $\{\mathbf{X}_n(\mu)\}$ converges to a limit, which we denote by $\mathbf{X}(\mu)$. This implies that:

$$\lim_{n\to\infty} \mathbf{X}_n(\mu) = \mathbf{X}(\mu).$$

And since $\mathbf{X}_{n+1}(\mu) = \mathbf{H}(\mathbf{X}_n(\mu))$, applying limits as $n \to \infty$ on both sides, and by the continuity of $\mathbf{H}$, we have

$$\lim_{n\to\infty} \mathbf{X}_{n+1}(\mu) = \lim_{n\to\infty} \mathbf{H}(\mathbf{X}_n(\mu)) = \mathbf{H}(\lim_{n\to\infty} \mathbf{X}_n(\mu)).$$

and

$$\mathbf{X}(\mu) = \mathbf{H}(\mathbf{X}(\mu)).$$

This implies that the limit $\mathbf{X}(\mu)$ is a fixed point of $\mathbf{H}$. Therefore, $\mathbf{X}(\mu)$ satisfies:

$$\mathbf{X}(\mu) = \mathbf{X}_0 + \frac{1}{\Gamma(\sigma)} \sum_{s=0}^{\mu-\sigma} (\mu - s - 1)^{\sigma-1} \mathbf{F}(\mu - 1 + \sigma,\ \mathbf{X}(\mu - 1 + \sigma)).$$

Thus, a recursive sequence of functions $\mathbf{X}_n(\mu)$ approaches the solution. This sequence converges to a unique function $\mathbf{X}(\mu)$, which represents the solution to the given system, according to the contraction mapping theorem. Therefore, a solution exists for the given system. □

3.5 *Hyers-Ulam stability*

We now investigate the Hyers-Ulam stability of the model. This type of stability is particularly important for models intended for clinical or numerical applications. It implies that if an approximate solution is found (for example, from numerical simulations with finite precision, or from noisy experimental data where measurements of viral load and T-cell counts have inherent error), there exists a true, exact solution to the model nearby. This provides critical confidence in the robustness of our model's predictions, ensuring that small deviations or uncertainties in initial conditions or parameter estimation do not lead to qualitatively different long-term outcomes.

Theorem 5 The model's stability is assessed in the Hyers-Ulam sense, as established by [44], provided that:

$$0 < \frac{k\Gamma(b + \sigma + 1)}{\Gamma(\sigma + 1)\Gamma(b + 1)} < 1.$$

Proof. Let $\mathbf{Y}, \mathbf{X} \in \mathbf{C}([0,\ T])$ be a solution of model (1). Then, we have

$$\begin{aligned} |\mathbf{H}(\mathbf{Y}(\mu)) - \mathbf{H}(\mathbf{X}(\mu))| = \Bigg| & \mathbf{Y}_0 + \frac{1}{\Gamma(\sigma)} \sum_{s=0}^{\mu-\sigma} (\mu - s - 1)^{\sigma-1} \mathbf{F}(\mu - 1 + \sigma, \mathbf{Y}(\mu - 1 + \sigma)) \\ & - \left(\mathbf{X}_0 + \frac{1}{\Gamma(\sigma)} \sum_{s=0}^{\mu-\sigma} (\mu - s - 1)^{\sigma-1} \mathbf{F}(\mu + \sigma - 1, \mathbf{X}(\mu - 1 + \sigma)) \right) \Bigg| \end{aligned} \tag{6}$$

$$\begin{aligned} \leq \frac{1}{\Gamma(\sigma)} \sum_{s=0}^{\mu-\sigma} (\mu - s - 1)^{\sigma-1} & |\mathbf{F}(\mu - 1 + \sigma, \mathbf{Y}(\mu - 1 + \sigma)) \\ & - \mathbf{F}(\mu - 1 + \sigma, \mathbf{X}(\mu - 1 + \sigma))|. \end{aligned} \tag{7}$$

By Theorem 3, $\mathbf{F}(\mu - 1 + \sigma,\ \mathbf{X}(\mu - 1 + \sigma))$ satisfies the Lipschitz condition $k = \max_{i=1}^{3} \{\mathscr{L}_{\mathbb{K}_i}\} > 0$. Then, we obtain that

$$\|\mathbf{H}(\mathbf{Y})-\mathbf{H}(\mathbf{X})\| \leq \frac{k\|\mathbf{Y}-\mathbf{X}\|}{\Gamma(\sigma)} \sum_{s=0}^{\mu-\sigma} (\mu-s-1)^{\sigma-1}.$$

The summation can be represented in terms of the Gamma function as follows

$$\|\mathbf{H}(\mathbf{Y})-\mathbf{H}(\mathbf{X})\| \leq \frac{k\Gamma(b+\sigma+1)}{\Gamma(\sigma+1)\Gamma(b+1)} \|\mathbf{Y}-\mathbf{X}\|. \tag{8}$$

Thus, by triangle inequality with the fact that $\|\mathbf{Y}-\mathbf{H}(\mathbf{Y})\| \leq \Upsilon > 0$ and equation (8), we have

$$\begin{aligned} \|\mathbf{Y}-\mathbf{X}\| &= \|\mathbf{Y}-\mathbf{H}(\mathbf{Y})+\mathbf{H}(\mathbf{Y})-\mathbf{X}\| \\ &\leq \|\mathbf{Y}-\mathbf{H}(\mathbf{Y})\| + \|\mathbf{H}(\mathbf{Y})-\mathbf{H}(\mathbf{X})\| \\ &\leq \Upsilon + \frac{k\Gamma(b+\sigma+1)}{\Gamma(\sigma+1)\Gamma(b+1)} \|\mathbf{Y}-\mathbf{X}\|. \end{aligned}$$

Consequently

$$\|\mathbf{Y}-\mathbf{X}\| \leq \frac{\Upsilon}{1-\left[\frac{k\Gamma(b+\sigma+1)}{\Gamma(\sigma+1)\Gamma(b+1)}\right]}.$$

Put $\Phi = \frac{1}{1-\left[\frac{k\Gamma(b+\sigma+1)}{\Gamma(\sigma+1)\Gamma(b+1)}\right]} > 0$ and $\Upsilon > 0$, then

$$\|\mathbf{Y}-\mathbf{X}\| \leq \Upsilon\Phi.$$

Thus, the model (1) is Hyers-Ulam stable. □

3.6 *Equilibrium points and basic reproduction number*

Equilibrium points are the steady-state solutions of the system, where the rates of change of all variables are zero. These points represent the long-term behavior of the infection and are found at the intersection of the system's nullclines. To find the equilibrium points, we set ${}^{C}\Delta^{\sigma}\mathbb{U}(\mu)=0$, ${}^{C}\Delta^{\sigma}\mathbb{I}(\mu)=0$, and ${}^{C}\Delta^{\sigma}\mathbb{V}(\mu)=0$ and solve the resulting system of algebraic equations:

$$\begin{cases} 0 = \tau - p\mathbb{U}(\mu-1+\sigma) + \varsigma\mathbb{U}(\mu-1+\sigma)\left(1 - \dfrac{\mathbb{U}(\mu-1+\sigma)}{\mathbb{U}_{\max}}\right) \\ \qquad - k\mathbb{V}(\mu-1+\sigma)\mathbb{U}(\mu-1+\sigma) + \delta\mathbb{I}(\mu-1+\sigma), \\ 0 = k\mathbb{V}(\mu-1+\sigma)\mathbb{U}(\mu+\sigma-1) - (\beta+\delta)\mathbb{I}(\mu-1+\sigma), \\ 0 = N\beta\mathbb{I}(\mu-1+\sigma) - \gamma\mathbb{V}(\mu-1+\sigma)\ . \end{cases} \tag{9}$$

From the second equation, we have

$$\mathbb{I}(\mu-1+\sigma) = \frac{k\mathbb{V}(\mu-1+\sigma)\mathbb{U}(\mu-1+\sigma)}{\beta+\delta}. \tag{10}$$

From the third equation, we have

$$\mathbb{V}(\mu-1+\sigma) = \frac{N\beta\mathbb{I}(\mu-1+\sigma)}{\gamma}. \tag{11}$$

Substituting the equation (10) into (11), we get

$$\mathbb{V}(\mu-1+\sigma) = N\beta\frac{k\mathbb{V}(\mu+\sigma-1)\mathbb{U}(\mu-1+\sigma)}{\gamma(\beta+\delta)}. \tag{12}$$

So

$$\mathbb{V}(\mu-1+\sigma)\left(1 - \frac{N\beta k}{\gamma(\beta+\delta)}\right) = 0. \tag{13}$$

The equation (13) gives us two possible scenarios:

• The Trivial Equilibrium (Disease-Free Equilibrium): $\mathbb{V}(\mu-1+\sigma) = 0$.

If $\mathbb{V}(\mu-1+\sigma) = 0$, then by the second equation in (9), we have $\mathbb{I}(\mu-1+\sigma) = 0$. Substituting $\mathbb{V}(\mu-1+\sigma) = 0$ and $\mathbb{I}(\mu-1+\sigma) = 0$ into the first equation in (9), we have:

$$0 = \tau - p\mathbb{U}(\mu-1+\sigma) + \varsigma\mathbb{U}(\mu-1+\sigma)\left(1 - \frac{\mathbb{U}(\mu-1+\sigma)}{\mathbb{U}_{\max}}\right).$$

Simplifying yields:

$$\frac{\varsigma}{\mathbb{U}_{\max}}\mathbb{U}^2(\mu-1+\sigma) - (\varsigma-p)\mathbb{U}(\mu-1+\sigma) - \tau = 0.$$

This is a quadratic equation in $\mathbb{U}$. Solving for $\mathbb{U}$ using the quadratic formula, we obtain:

$$\mathbb{U}(\mu-1+\sigma)=\frac{(\varsigma-p)\pm\sqrt{(\varsigma-p)^2+4\left(\frac{\varsigma}{\mathbb{U}_{\max}}\right)(\tau)}}{2\left(\frac{\varsigma}{\mathbb{U}_{\max}}\right)}$$

$$=\frac{\mathbb{U}_{\max}}{2\varsigma}\left[(\varsigma-p)\pm\sqrt{(\varsigma-p)^2+\frac{4\varsigma\tau}{\mathbb{U}_{\max}}}\right].$$

Since $\mathbb{U}$ must be non-negative, we take the positive root. Therefore, the disease-free equilibrium point is given by:

$$E_0=\left(\frac{\mathbb{U}_{\max}}{2\varsigma}\left[(\varsigma-p)+\sqrt{(\varsigma-p)^2+\frac{4\varsigma\tau}{\mathbb{U}_{\max}}}\right],\ 0,\ 0\right).$$

• The Infected Equilibrium (Endemic Equilibrium):

If $\mathbb{V}(\mu-1+\sigma)\neq 0$, then equation (13) gives $1=\frac{N\beta k}{\gamma(\beta+\delta)}$ or $\frac{\gamma(\beta+\delta)}{N\beta k}=1$. This equation defines the basic reproduction number (R_0). If $R_0=\frac{N\beta k}{\gamma(\beta+\delta)}>1$, an infected equilibrium may exist. Let's call $R_0=\frac{N\beta k}{\gamma(\beta+\delta)}$. Then $\gamma(\beta+\delta)=N\beta k$ and $\gamma=\frac{N\beta k}{(\beta+\delta)}$. From the second equation in (9), we have

$$\mathbb{I}(\mu-1+\sigma)=\frac{k\mathbb{V}(\mu-1+\sigma)\mathbb{U}(\mu-1+\sigma)}{\beta+\delta}. \tag{14}$$

From the third equation in (9), we have

$$\mathbb{V}(\mu-1+\sigma)=\frac{N\beta\mathbb{I}(\mu-1+\sigma)}{\gamma}. \tag{15}$$

Substituting equation (14) into equation (15), we get:

$$\mathbb{V}(\mu-1+\sigma)=\frac{N\beta}{\gamma}\frac{k\mathbb{V}(\mu-1+\sigma)\mathbb{U}(\mu-1+\sigma)}{\beta+\delta}=\frac{N\beta k}{\gamma(\beta+\delta)}\mathbb{V}(\mu-1+\sigma)\mathbb{U}(\mu-1+\sigma).$$

Substituting $\gamma=\frac{N\beta k}{(\beta+\delta)}$ we get $\mathbb{U}(\mu-1+\sigma)=1$. So, at the endemic equilibrium, $\mathbb{U}>0$, $\mathbb{V}>0$, $\mathbb{U}=1$. Thus $\mathbb{U}=1$. Now we can write

$$\mathbb{I}=\frac{k\mathbb{V}(\mu-1+\sigma)}{\beta+\delta}.$$

Substituting $\mathbb{U}=1$ into the first equation:

$$0 = \tau - p + \varsigma\left(1 - \frac{1}{\mathbb{U}_{\max}}\right) - k\mathbb{V} + \delta\mathbb{I}.$$

Substituting $\mathbb{I} = \dfrac{k\mathbb{V}(\mu - 1 + \sigma)}{\beta + \delta}$, we have

$$0 = \tau - p + \varsigma\left(1 - \frac{1}{\mathbb{U}_{\max}}\right) - k\mathbb{V}(\mu + \sigma - 1) + \delta\frac{k\mathbb{V}(\mu - 1 + \sigma)}{\beta + \delta}.$$

Solving for $\mathbb{V}$ yields:

$$\mathbb{V} = \frac{\tau - p + \varsigma\left(1 - \dfrac{1}{\mathbb{U}_{\max}}\right)}{k\left(\dfrac{\beta}{\beta + \delta}\right)} = \frac{(\beta + \delta)\left[\tau - p + \varsigma\left(1 - \dfrac{1}{\mathbb{U}_{\max}}\right)\right]}{k\beta}.$$

For $\mathbb{V} > 0$, we require $\tau + \varsigma\left(1 - \dfrac{1}{\mathbb{U}_{\max}}\right) > p$, as before. Now, substituting this expression for $\mathbb{V}$ into the equation for $\mathbb{I}$, we get:

$$\mathbb{I} = \frac{k}{\beta + \delta}\left(\frac{(\beta + \delta)\left[\tau - p + \varsigma\left(1 - \dfrac{1}{\mathbb{U}_{\max}}\right)\right]}{k\beta}\right) = \frac{\tau - p + \varsigma\left(1 - \dfrac{1}{\mathbb{U}_{\max}}\right)}{\beta}.$$

So the endemic equilibrium is:

$$E_* = \left(1, \frac{\tau - p + \varsigma\left(1 - \dfrac{1}{\mathbb{U}_{\max}}\right)}{\beta}, \frac{(\beta + \delta)\left[\tau - p + \varsigma\left(1 - \dfrac{1}{\mathbb{U}_{\max}}\right)\right]}{k\beta}\right).$$

An important feature of this model is that the basic reproduction number, R_0, does not explicitly depend on the fractional-order parameter σ. This implies that while the memory of the system (σ) profoundly affects the transient dynamics, it does not alter the fundamental threshold condition for an epidemic to occur.

4. Sensitivity analysis of the basic reproduction number

To effectively manage and potentially eradicate HIV, it is essential to understand the quantitative relationships between the model's parameters and the basic reproduction number (R_0), a key indicator of the infection's transmissibility. A sensitivity analysis serves this purpose by assessing the degree to which changes in individual parameters affect R_0. This allows us to prioritize interventions that target the parameters with the highest sensitivity indices, maximizing the impact

on controlling or eliminating the infection. The Sensitivity index (SEN), representing the relative change in R_0 due to a change in parameter $\mathscr{P}$, is expressed as:

$$\text{SEN}_{\mathscr{P}}^{R_0} = \frac{\mathscr{P}}{R_0}\frac{\partial R_0}{\partial \mathscr{P}}, \tag{16}$$

Now, we calculate the sensitivity index for each parameter $\mathscr{P} \in \{N,\ \beta,\ k,\ \gamma,\ \delta\}$ as follows:

- $\text{SEN}_N^{R_0} = \dfrac{N}{R_0}\dfrac{\partial R_0}{\partial N} = \dfrac{N}{\frac{N\beta k}{\gamma(\beta+\delta)}}\dfrac{\beta k}{\gamma(\beta+\delta)} = 1.$
- $\text{SEN}_\beta^{R_0} = \dfrac{\beta}{R_0}\dfrac{\partial R_0}{\partial \beta} = \dfrac{\beta}{\frac{N\beta k}{\gamma(\beta+\delta)}}\dfrac{Nk\delta}{\gamma(\beta+\delta)^2} = 0.5556.$
- $\text{SEN}_k^{R_0} = \dfrac{k}{R_0}\dfrac{\partial R_0}{\partial k} = \dfrac{k}{\frac{N\beta k}{\gamma(\beta+\delta)}}\dfrac{N\beta}{\gamma(\beta+\delta)} = 1.$
- $\text{SEN}_\gamma^{R_0} = \dfrac{\gamma}{R_0}\dfrac{\partial R_0}{\partial \gamma} = \dfrac{\gamma}{\frac{N\beta k}{\gamma(\beta+\delta)}}\left(-\dfrac{N\beta k}{\gamma^2(\beta+\delta)}\right) = -1.$
- $\text{SEN}_\delta^{R_0} = \dfrac{\delta}{R_0}\dfrac{\partial R_0}{\partial \delta} = \dfrac{\delta}{\frac{N\beta k}{\gamma(\beta+\delta)}}\left(-\dfrac{N\beta k}{\gamma(\beta+\delta)^2}\right) = -0.5556.$

The summary of sensitivity indices is presented in Table 4. In Figure 2, we present the bar chart of the sensitivity indices of the basic reproduction number (R_0) with respect to the most influential model parameters, based on the values in Table 4.

Table 4. Sensitivity Indices of R_0 with respect to model parameters

Parameter	Sensitivity index
N	1
β	0.473
k	1
γ	-1
δ	-0.527

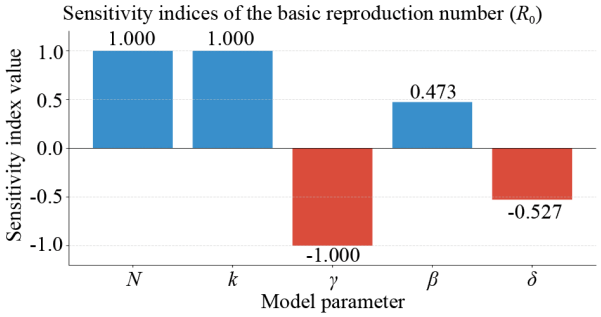


Figure 2. Bar chart of the sensitivity indices of the basic reproduction number (R_0) with respect to the most influential model parameters

Based on the values in Table 4 and Figure 2. The analysis reveals that the viral production rate (N), infection rate (k), and viral clearance rate (γ) have the strongest impact (indices of + 1, + 1, and -1, respectively), identifying them as

primary targets for intervention strategies. A positive index indicates that increasing the parameter increases R_0, while a negative index indicates the opposite.

In the Figure 3 and Figure 4, we present the contour 2D plots and contour 3D plots, respectively, for illuminating R_0 sensitivity to the joint parameter changes of the discrete fractional order of the HIV model.

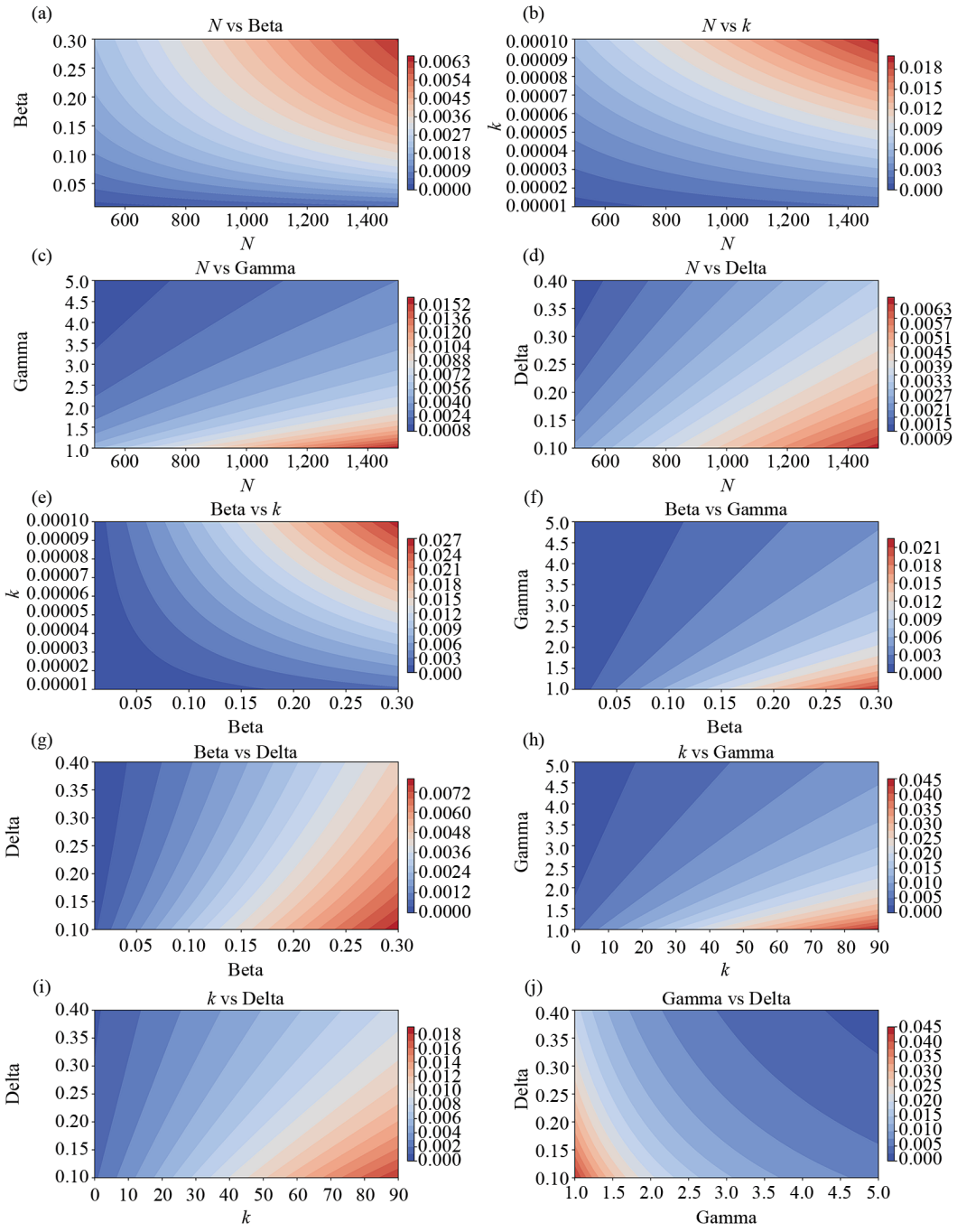


Figure 3. Contour 2D plots illustrating the value of the basic reproduction number, R_0, under joint variations of key model parameters

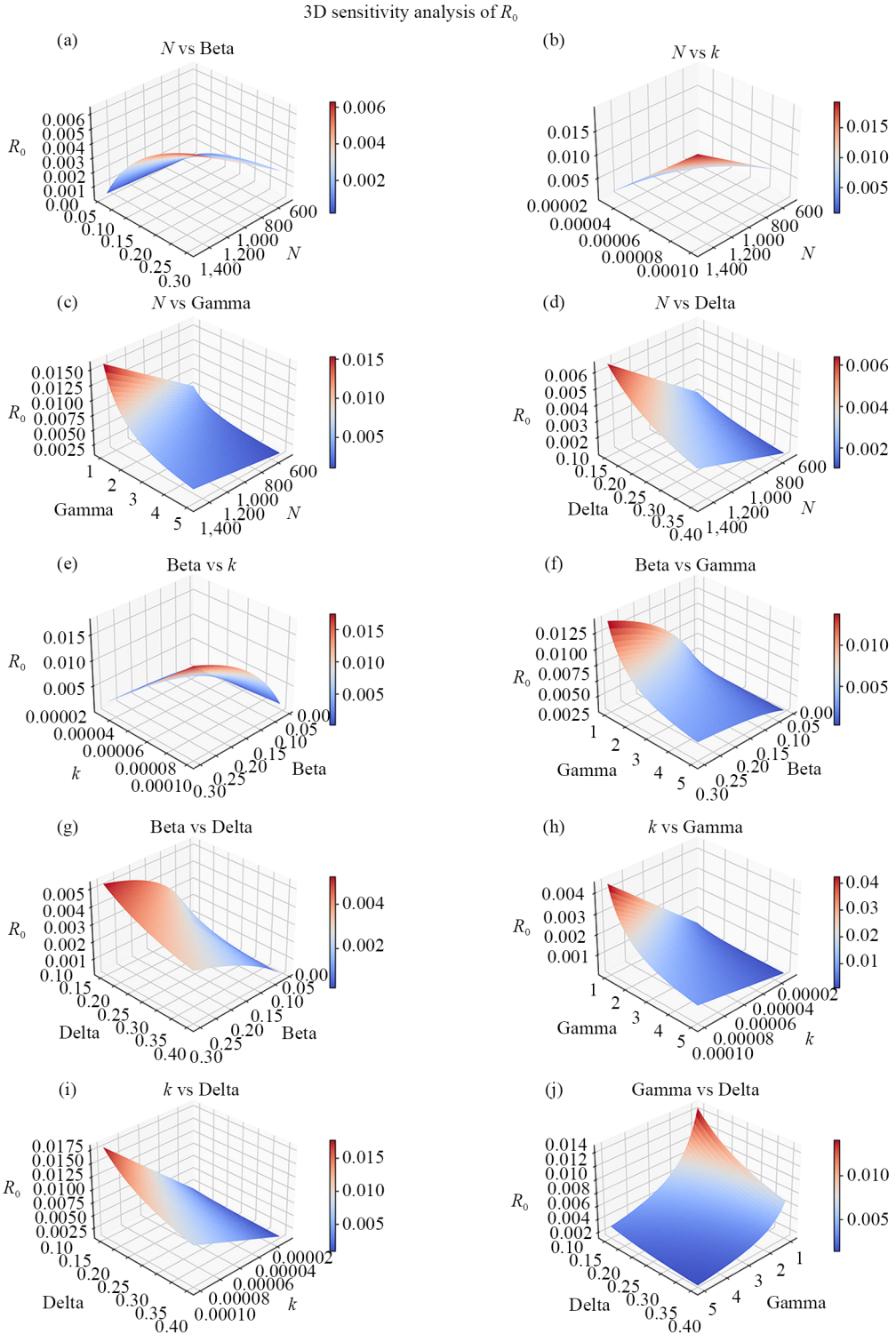


Figure 4. Contour 3D plots illustrating the value of the basic reproduction number, R_0, under joint variations of key model parameters

4.1 *Strategic insights from visual sensitivity analysis*

While the sensitivity indices in Table 4 identify which parameters are most influential, the contour plots in Figures 3 and 4 translate this theoretical knowledge into a practical framework for designing and optimizing intervention strategies. These visualizations facilitate a transition from abstract parameter sensitivity to concrete clinical decision-making, as illustrated in the following scenarios:

• **Designing Combination Therapies through Quantitative Trade-offs:** The contour plots serve as a strategic map for determining the required efficacy of mono- or combination therapies. Consider a hypothetical patient with a high viral production rate ($N = 1,200$) and a moderate viral clearance rate ($\gamma = 2.5$). Figure 3 places this patient in a high-risk region ($R_0 > 1$), indicating an uncontrolled infection. To achieve control ($R_0 < 1$, the blue zone), the model visually delineates several strategic pathways:

- **Strategy A (Aggressive Monotherapy):** A potent antiretroviral regimen, such as a protease inhibitor, could be deployed to drastically suppress viral production. The plot indicates that reducing N to below 800, while maintaining γ at 2.5, would suffice. This represents a high-intensity, virus-targeted approach.

- **Strategy B (Immunotherapy-Augmented Strategy):** An intervention designed to enhance immune clearance could be employed. To achieve control, γ would need to be increased above 4.0 without a reduction in N.

- **Strategy C (Optimized Combination Therapy):** The plots demonstrate the potential of a synergistic, combined approach. A moderate reduction of N to 1,000 (achievable with standard-dose antivirals) coupled with a moderate increase in γ to 3.5 (via an immunostimulant adjuvant) would also transition the patient into the controlled zone. This strategy may offer a superior therapeutic index by balancing efficacy with reduced potential for toxicity.

• **Identifying the Most Efficient Intervention Pathways:** The gradient of the response surfaces in Figure 4 provides a direct visual measure of intervention **leverage**. The pronounced decline in R_0 with small reductions in N or k indicates that therapies targeting viral production and cell infection are highly efficient; a minimal therapeutic effort yields a substantial reduction in viral replicative potential. Conversely, a shallower gradient for other parameters would indicate lower efficiency, requiring more significant changes for a comparable effect, thus rendering them less favorable as primary intervention targets.

In summary, the sensitivity analysis provides a validated roadmap for prioritizing intervention targets. The high positive sensitivity indices for the viral production rate (N) and infection rate (k) (SEN = 1) unequivocally identify them as the most potent leverage points for control. This finding provides a mathematical foundation for the mechanisms of established antiretroviral therapies:

• **Protease Inhibitors** and **Reverse Transcriptase Inhibitors** primarily act by reducing N (the number of infectious virions produced per cell).

• **Entry and Fusion Inhibitors** directly target k (the rate of successful cell infection).

Furthermore, the high negative sensitivity of the viral clearance rate (γ) (SEN $= -1$) highlights the potential efficacy of novel strategies aimed at boosting the host's innate or adaptive immune response to clear free virus particles. The negative sensitivity of the latency transition rate (δ) intriguingly suggests that therapeutic strategies promoting a latent state could, in theory, reduce the pool of productively infected cells and help contain viral replication.

4.2 *Limitations*

It's crucial to remember that this sensitivity analysis is local, performed at a specific point in the parameter space. The specific numerical values of the sensitivity indices depend on the parameter values used in the model. A global sensitivity analysis, which evaluates sensitivity over the entire parameter space using methods like Latin Hypercube Sampling (LHS), would provide more robust insights and is a direction for future work. Furthermore, this analysis only considers direct effects on R_0 and does not account for potential indirect effects or complex interactions within the full biological system.

5. Stability analysis

5.1 *Stability of the disease-free equilibrium (E_0)*

To determine the local stability of the equilibrium points, we linearize the discrete system around each equilibrium. This involves finding the Jacobian matrix and analyzing its eigenvalues. The Jacobian matrix, J, is given by:

$$J = \begin{pmatrix} -p+\varsigma-\dfrac{2\varsigma\mathbb{U}}{\mathbb{U}_{\max}}-k\mathbb{V} & \delta & -k\mathbb{U} \\ k\mathbb{V} & -(\beta+\delta) & k\mathbb{U} \\ 0 & N\beta & -\gamma \end{pmatrix}$$

Substituting the coordinates of E_0 into the Jacobian matrix, we obtain:

$$J(E_0) = \begin{pmatrix} -p+\varsigma-\dfrac{2\varsigma\mathbb{U}_0}{\mathbb{U}_{\max}} & \delta & -k\mathbb{U}_0 \\ 0 & -(\beta+\delta) & k\mathbb{U}_0 \\ 0 & N\beta & -\gamma \end{pmatrix}$$

Where

$$\mathbb{U}_0 = \frac{\mathbb{U}_{\max}}{2\varsigma}\left[(\varsigma-p)+\sqrt{(\varsigma-p)^2+\frac{4\varsigma\tau}{\mathbb{U}_{\max}}}\right].$$

The eigenvalues of this matrix determine the local stability of E_0. The eigenvalues are the solutions of the characteristic equation

$$\det(J(E_0)-\lambda I)=0.$$

Which gives us:

$$\left(-p+\varsigma-\frac{2\varsigma\mathbb{U}_0}{\mathbb{U}_{\max}}-\lambda\right)[(-(\beta+\delta)-\lambda)(-\gamma-\lambda)-N\beta k\mathbb{U}_0]=0$$

This will result in three eigenvalues,

$$\lambda_1 = -p+\varsigma-\frac{2\varsigma\mathbb{U}_0}{\mathbb{U}_{\max}},$$

where stability requires $\lambda_1<0$, which corresponds to the condition $p>\varsigma(1-2\mathbb{U}_0/\mathbb{U}_{\max})$, and λ_2 and λ_3 will come from solving

$$(-(\beta+\delta)-\lambda)(-\gamma-\lambda)-N\beta k\mathbb{U}_0=0$$

which is a quadratic equation. The disease-free equilibrium is stable if $\lambda_1 < 0$, λ_2 and λ_3 are negative or have negative real parts. Rearrange for λ_2 and λ_3. We have

$$\lambda^2 + (\beta + \delta + \gamma)\lambda + (\beta + \delta)\gamma - k\mathbb{U}_0 N\beta = 0.$$

Using the quadratic equation, we get:

$$\lambda = \frac{-(\beta + \delta + \gamma) \pm \sqrt{(\gamma - (\beta + \delta))^2 + 4k\mathbb{U}_0 N\beta}}{2}.$$

If $\dfrac{N\beta k}{\gamma(\beta + \delta)} < 1$, i.e. $R_0 < 1$, and $\lambda_1 < 0$, the disease-free equilibrium point (E_0) is locally asymptotically stable.

5.2 *Stability of the endemic equilibrium (E_*)*

Now consider the Endemic Equilibrium

$$E_* = \left(1,\ \frac{\tau - p + \varsigma\left(1 - \dfrac{1}{\mathbb{U}_{\max}}\right)}{\beta},\ \frac{(\beta + \delta)\left[\tau - p + \varsigma\left(1 - \dfrac{1}{\mathbb{U}_{\max}}\right)\right]}{k\beta} \right).$$

The Jacobian is given by

$$J = \begin{pmatrix} -p + \varsigma - \dfrac{2\varsigma\mathbb{U}}{\mathbb{U}_{\max}} - k\mathbb{V} & \delta & -k\mathbb{U} \\ k\mathbb{V} & -(\beta + \delta) & k\mathbb{U} \\ 0 & N\beta & -\gamma \end{pmatrix}.$$

Substituting the coordinates of E_* into the Jacobian matrix, we obtain

$$J(E_*) = \begin{pmatrix} -p + \varsigma - \dfrac{2\varsigma}{\mathbb{U}_{\max}} - k\overline{\mathbb{V}} & \delta & -k \\ k\overline{\mathbb{V}} & -(\beta + \delta) & k \\ 0 & N\beta & -\gamma \end{pmatrix}.$$

Where

$$\overline{\mathbb{V}} = \frac{(\beta + \delta)\left[\tau - p + \varsigma\left(1 - \dfrac{1}{\mathbb{U}_{\max}}\right)\right]}{k\beta}.$$

Let's define the quantity $A = -p + \varsigma - \dfrac{2\varsigma}{\mathbb{U}_{\max}} - k\overline{\mathbb{V}}$. Substituting, we have

$$A = -p + \varsigma - \frac{2\varsigma}{\mathbb{U}_{\max}} - \frac{(\beta+\delta)\left[\tau - p + \varsigma\left(1 - \frac{1}{\mathbb{U}_{\max}}\right)\right]}{\beta}.$$

The characteristic equation is then given by $\det(J(E_*) - \lambda I) = 0$. Then, we have

$$\begin{vmatrix} A-\lambda & \delta & -k \\ k\overline{\mathbb{V}} & -(\beta+\delta)-\lambda & k \\ 0 & N\beta & -\gamma-\lambda \end{vmatrix} = 0.$$

Thus, we have

$$\lambda^3 + G\lambda^2 + D\lambda + W = 0,$$

where

$$G = A + \beta + \delta + \gamma,$$

$$D = A(\beta + \delta + \gamma) + k\delta\overline{\mathbb{V}},$$

$$W = k\gamma\delta\overline{\mathbb{V}} + k(\beta+\delta)\gamma k\overline{\mathbb{V}} = k^2\beta\delta.$$

We noted that all coefficients of the characteristic polynomial are positive, i.e., $G > 0,\ D > 0,\ W > 0$. The Routh-Hurwitz stability condition requires $GD - W > 0$. Evaluating this at the endemic equilibrium where $U = U^* = 1$, the condition becomes stable if

$$\frac{2\varsigma}{U_{\max}} + p - \varsigma > 0.$$

5.3 *Biological interpretation of stability results*

The stability of the two equilibria provides critical clinical insights into the long-term outcomes of HIV infection:

• Disease-Free Equilibrium (E_0): The stability of E_0 when the basic reproduction number $R_0 < 1$ corresponds to a scenario where the infection is cleared by the host. Clinically, this represents either a failed transmission or an infection that is successfully suppressed by the immune system before it can become established. Our analysis shows that this state is locally asymptotically stable under this condition, meaning small viral introductions will be eliminated.

• Endemic Equilibrium (E_*): The stability of E_* when $R_0 > 1$ represents a chronic, persistent infection. In this state, the virus is not cleared, and the populations of T-cells and virus stabilize at a steady, non-zero level. This corresponds directly to the chronic phase of HIV, where the viral load remains relatively constant for years. Our analysis confirms that this state is stable, providing a mathematical basis for the persistence of the virus in an infected individual.

5.4 *Bifurcation analysis*

To delve deeper into the model's dynamics, particularly at the epidemic threshold, we perform a bifurcation analysis on the underlying model (1). This analysis helps determine the nature of the bifurcation at $R_0 = 1$ and reveals whether complex behaviors, such as a backward bifurcation, are possible. A backward bifurcation, where a stable endemic state can persist even when $R_0 < 1$, has significant implications for disease control, suggesting that merely satisfying the $R_0 < 1$ condition may not be sufficient for eradication.

We employ the center manifold theory as described by Castillo-Chavez and Song [45]. Let us select the infection rate, k, as the primary bifurcation parameter. The basic reproduction number is given by $R_0 = \dfrac{N\beta k\mathbb{U}_0}{\gamma(\beta+\delta)}$. The critical value $k = k^*$ at which a bifurcation may occur is found by setting $R_0 = 1$:

$$k^* = \frac{\gamma(\beta+\delta)}{N\beta\mathbb{U}_0}, \tag{17}$$

where $\mathbb{U}_0$ is the stable disease-free level of uninfected T-cells.

Let the state variables be $x_1 = \mathbb{U},\ x_2 = \mathbb{I},\ x_3 = \mathbb{V}$. The system of equations (1) can be written as ${}^{C}\Delta^{\sigma}x_i(\mu) = f_i(x_1,\ x_2,\ x_3)$. We evaluate the Jacobian matrix, J, at the disease-free equilibrium $E_0 = (\mathbb{U}_0,\ 0,\ 0)$ with the critical parameter value $k = k^*$.

$$J(E_0,\ k^*) = \begin{pmatrix} -p+\varsigma\left(1-\dfrac{2\mathbb{U}_0}{\mathbb{U}_{\max}}\right) & \delta & -k^*\mathbb{U}_0 \\ 0 & -(\beta+\delta) & k^*\mathbb{U}_0 \\ 0 & N\beta & -\gamma \end{pmatrix}. \tag{18}$$

At $k = k^*$, this Jacobian has a simple zero eigenvalue. We now compute the left and right eigenvectors, $\mathbf{v}$ and $\mathbf{w}$, corresponding to this zero eigenvalue. The right eigenvector $\mathbf{w} = (w_1,\ w_2,\ w_3)^T$ is found by solving $J(E_0,\ k^*)\mathbf{w} = \mathbf{0}$. This yields:

$$w_1 = -\frac{\delta\gamma + k^*\mathbb{U}_0N\beta}{-p+\varsigma\left(1-\dfrac{2\mathbb{U}_0}{\mathbb{U}_{\max}}\right)}w_2 = -\frac{\delta(\beta+\delta)}{-p+\varsigma\left(1-\dfrac{2\mathbb{U}_0}{\mathbb{U}_{\max}}\right)}\frac{\gamma}{k^*\mathbb{U}_0}w_3, \quad w_2 = \frac{\gamma}{k^*\mathbb{U}_0}w_3. \tag{19}$$

Setting $w_3 > 0$, we have $w_2 > 0$ and $w_1 < 0$, which is biologically expected as an increase in infected cells corresponds to a decrease in healthy cells. The left eigenvector $\mathbf{v} = (v_1,\ v_2,\ v_3)$ is found by solving $\mathbf{v}J(E_0,\ k^*) = \mathbf{0}$. This gives $v_1 = 0$, and:

$$v_2 = \frac{\gamma}{N\beta}v_3. \tag{20}$$

We choose $v_3 > 0$, which implies $v_2 > 0$. The direction of the bifurcation is determined by the signs of two coefficients, a and b. According to the theory in [45], a backward bifurcation occurs if $a > 0$ and $b > 0$. The coefficient a is computed from the second-order derivatives of the system functions f_i:

$$a = \sum_{i,\ j,\ l=1}^{3} v_i w_j w_l \frac{\partial^2 f_i}{\partial x_j \partial x_l}(E_0,\ k^*), \tag{21}$$

The relevant non-zero second derivatives of our system, evaluated at E_0, are:

$$\frac{\partial^2 f_1}{\partial \mathbb{U}^2} = -\frac{2\varsigma}{\mathbb{U}_{\max}},$$

$$\frac{\partial^2 f_1}{\partial \mathbb{U} \partial \mathbb{V}} = -k^*,$$

$$\frac{\partial^2 f_2}{\partial \mathbb{U} \partial \mathbb{V}} = k^*.$$

Since $v_1 = 0$, the only terms contributing to a come from f_2.

$$a = v_2 \left(2 w_1 w_3 \frac{\partial^2 f_2}{\partial \mathbb{U} \partial \mathbb{V}} \right) = 2 v_2 w_1 w_3 k^*. \tag{22}$$

Given that $v_2 > 0$, $w_3 > 0$, $k^* > 0$, the sign of a depends on the sign of w_1. As we established $w_1 < 0$, we have:

$$a < 0. \tag{23}$$

The coefficient b is given by:

$$b = \sum_{i,j=1}^{3} v_i w_j \frac{\partial^2 f_i}{\partial x_j \partial k}(E_0,\ k^*). \tag{24}$$

The required second derivatives are:

$$\frac{\partial^2 f_1}{\partial \mathbb{U} \partial k} = -\mathbb{V}\Big|_{E_0} = 0,$$

$$\frac{\partial^2 f_2}{\partial \mathbb{U} \partial k} = \mathbb{V}\Big|_{E_0} = 0,$$

$$\frac{\partial^2 f_2}{\partial \mathbb{V} \partial k} = \mathbb{U}\Big|_{E_0} = \mathbb{U}_0.$$

Therefore, the sum for b simplifies to:

$$b = v_2 \left(w_3 \frac{\partial^2 f_2}{\partial \mathbb{V} \partial k} \right) = v_2 w_3 \mathbb{U}_0. \tag{25}$$

Since $v_2 > 0$, $w_3 > 0$, and $\mathbb{U}_0 > 0$, we definitively have $b > 0$. Since $a < 0$ and $b > 0$, the condition for a backward bifurcation ($a > 0$) is not met. Therefore, our analysis reveals that the model exhibits a standard forward bifurcation at $R_0 = 1$. This implies that, for the dynamics governed by the model, the disease-free equilibrium is locally asymptotically stable whenever $R_0 < 1$, and an unstable endemic equilibrium emerges for $R_0 > 1$. This finding reinforces the role of R_0 as the definitive critical threshold for controlling HIV infection within this modeling framework.

6. Numerical solution and discussion

Having established the theoretical existence of a solution, we now turn to numerical methods to approximate and visualize the model's behavior for specific parameter values. To simulate the dynamics of the discrete fractional-order model (1), we employ a numerical scheme derived directly from the equivalent fractional-sum equation (2). This method is a standard approach for solving Caputo-type fractional difference equations [31, 46] and can be seen as a discrete analog of the fractional Adams method for continuous systems. While a formal convergence analysis is beyond the scope of this theoretical study, the scheme's structure ensures that it reduces to the exact solution for the integer-order case ($\sigma = 1$) and is consistent with the broader class of fractional finite difference and spline methods used for solving complex dynamical systems [37, 40] For $\mu \in [0,\ b]_{\mathbb{N}_0}$, the model (1) is represented as follows:

$$\begin{aligned}
\mathbb{U}(n) = \mathbb{U}(0) + \frac{1}{\Gamma(\sigma)} \sum_{s=1-\sigma}^{n-\sigma} (n-s-1)^{\sigma-1} \big[& \tau - p\mathbb{U}(n+\sigma-1) \\
& + \varsigma \mathbb{U}(n+\sigma-1) \left(1 - \frac{\mathbb{U}(n+\sigma-1)}{\mathbb{U}_{\max}} \right) \\
& - k\mathbb{V}(n+\sigma-1)\mathbb{U}(n+\sigma-1) + \delta \mathbb{I}(n+\sigma-1) \big],
\end{aligned} \tag{26}$$

$$\begin{aligned}
\mathbb{I}(n) = \mathbb{I}(0) + \frac{1}{\Gamma(\sigma)} \sum_{s=1-\sigma}^{n-\sigma} & (n-s-1)^{\sigma-1} \\
& \times \big[k\mathbb{V}(n+\sigma-1)\mathbb{U}(n+\sigma-1) - (\beta+\delta)\mathbb{I}(n+\sigma-1) \big],
\end{aligned} \tag{27}$$

and

$$\mathbb{V}(n) = \mathbb{V}(0) + \frac{1}{\Gamma(\sigma)} \sum_{s=1-\sigma}^{n-\sigma} (n-s-1)^{\sigma-1} \big[N\beta\mathbb{I}(n+\sigma-1) - \gamma\mathbb{V}(n+\sigma-1) \big]. \tag{28}$$

Since $(n-s-1)^{\sigma-1} = \dfrac{\Gamma(n-s)}{\Gamma(n+1-s-\sigma)}$ and for $s+\sigma-1 = j$, then the numerical equations (26)-(28) can be designed for $\sigma \in (0,\ 1]$, $n = 1,\ 2,\ \ldots$ as follows

$$\mathbb{U}(n) = \mathbb{U}(0) + \frac{1}{\Gamma(\sigma)} \sum_{j=0}^{n-1} \frac{\Gamma(n-j-1+\sigma)}{\Gamma(n-1)} \left[\tau - p\mathbb{U}(j) + \varsigma \mathbb{U}(j) \left(1 - \frac{\mathbb{U}(j)}{\mathbb{U}_{\max}} \right) - k\mathbb{V}(j)\mathbb{U}(j) + \delta \mathbb{I}(j) \right],$$

$$\mathbb{I}(n) = \mathbb{I}(0) + \frac{1}{\Gamma(\sigma)} \sum_{j=0}^{n-1} \frac{\Gamma(n-j-1+\sigma)}{\Gamma(n-1)} \left[k\mathbb{V}(j)\mathbb{U}(j) - (\beta + \delta)\mathbb{I}(j) \right],$$

and

$$\mathbb{V}(n) = \mathbb{V}(0) + \frac{1}{\Gamma(\sigma)} \sum_{j=0}^{n-1} \frac{\Gamma(n-j-1+\sigma)}{\Gamma(n-1)} \left[N\beta \mathbb{I}(j) - \gamma \mathbb{V}(j) \right].$$

7. Simulations and discussion

In this part, we plot the graphs of $\mathbb{U}$ Figure 5, $\mathbb{I}$ Figure 6, and $\mathbb{V}$ Figure 7 with high fractional order $\sigma = 0.6, 0.7, 0.8, 0.9, 1$.

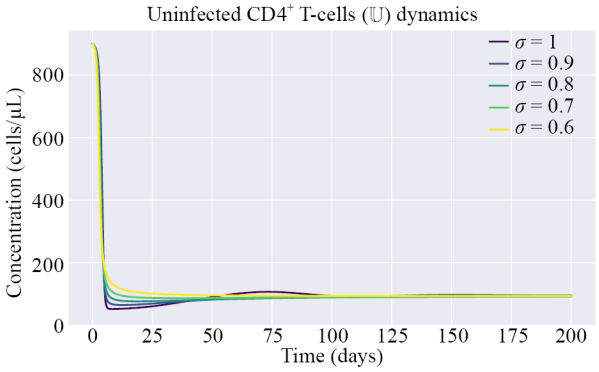


Figure 5. Simulation of uninfected CD4$^+$ T-cell dynamics, $\mathbb{U}$, for different fractional orders (σ). Biologically, a lower σ (stronger memory) results in a less severe initial decline but a worse long-term recovery, suggesting that the 'memory' of initial infection impairs the immune system's regenerative capacity

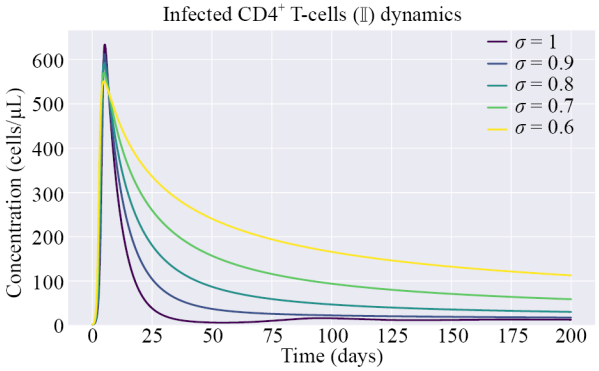


Figure 6. Simulation of actively infected CD4$^+$ T-cell dynamics, $\mathbb{I}$, for different fractional orders (σ)

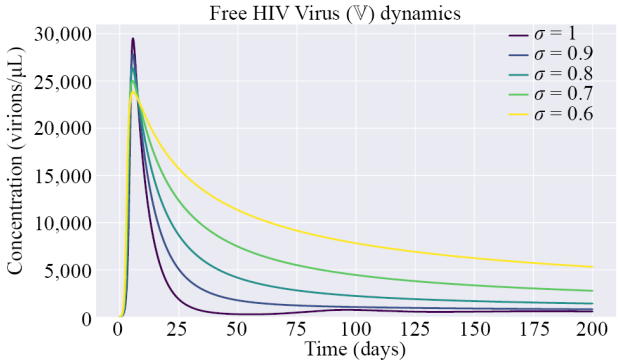


Figure 7. Simulation of free virus dynamics, $\mathbb{V}$, for different fractional orders (σ)

7.1 *Discussion of temporal dynamics and the influence of fractional order*

The time series analyses presented in Figures 5-7 reveal dynamics that are highly consistent with the clinical progression of HIV, while also highlighting the profound and nuanced influence of the fractional order σ, which serves as an index of the system's memory.

• **Uninfected CD4$^+$ T-cell Dynamics Figure 5:** Figure 5 shows the concentration of healthy CD4$^+$ T-cells ($\mathbb{U}$). All simulations exhibit an initial rapid decline, mirroring the T-cell depletion characteristic of the acute phase of HIV. The fractional order σ reveals a critical trade-off:

- **Initial Decline:** The rate of depletion is strongly dependent on σ. The integer-order case ($\sigma = 1$, representing a memoryless system) shows the most rapid and severe initial drop. As σ decreases (i.e., as system memory strengthens), the initial decline becomes progressively slower and less steep, indicating a dampened response to the initial infection shock.

- **Long-Term Outcome:** Counterintuitively, a stronger memory leads to a worse long-term outcome. The final endemic equilibrium level of healthy T-cells is lowest for the strongest memory case ($\sigma = 0.6$) and highest for the memoryless case ($\sigma = 1$). This suggests that while a stronger memory buffer the initial infection shock, it also leads to a persistent "memory" of cumulative damage, resulting in a more severe chronic state of immunodeficiency and impaired regenerative capacity.

• **Infected Cells and Free Virus Dynamics Figures 6 and 7:** Figures 6 and 7 show the dynamics of actively infected T-cells ($\mathbb{I}$) and free virus particles ($\mathbb{V}$). Their behavior is qualitatively similar and provides a clear picture of the infection's progression:

- **Acute Phase Burst:** Both populations exhibit a sharp initial spike, peaking within the first 25 days. This burst corresponds to the high viral load (viremia) observed during acute HIV infection. The magnitude of this peak is modulated by memory: the $\sigma = 1$ case (weakest memory) produces the highest and sharpest peak. Lower values of σ (stronger memory) effectively dampen this initial burst, resulting in a lower and broader peak.

- **Chronic Phase Stabilization:** Following the peak, the system settles into a stable endemic equilibrium, representing the chronic phase of HIV where the viral load stabilizes at a "set point". Crucially, this chronic set point is highest for the strongest memory case ($\sigma = 0.6$) and lowest for the weakest memory case ($\sigma = 1$).

• **Synthesis: The Competing Effects of Memory and Temporal Scaling**

Taken together, these results provide a crucial insight: the fractional order σ introduces a fundamental trade-off between the acute and chronic phases of HIV infection. A stronger memory (lower σ) is beneficial during the acute phase, as it mitigates the initial T-cell loss and viral burst. However, this benefit comes at the cost of a worse chronic outcome, characterized by a lower long-term healthy T-cell count and a higher viral set point.

This nuanced behavior, where the system's historical states continuously influence its future trajectory, cannot be captured by traditional integer-order models. The fractional-order framework inherently incorporates **temporal scaling**, effectively modeling the long-tailed, non-Markovian dynamics prevalent in biological systems. These include the

extended lifespans and slow turnover of T-cell subsets, the delayed reactivation from latent reservoirs, and the cumulative nature of immune dysregulation. The competing effects of memory-providing an initial buffer at the expense of long-term pathology-offer a mathematical basis for the clinical observation that a severe initial infection can predict faster disease progression, suggesting that the immune system retains a damaging 'memory' of the initial immunologic insult.

7.2 *Comparative analysis with existing HIV models*

To contextualize our contribution, Table 3 contrasts key features of our model with established works in the literature. Unlike the continuous ODE models of Perelson [41], which lack memory effects, or the continuous fractional models of [9, 43], which are not framed for discrete data, our model uniquely synthesizes a discrete-time framework, fractional-order dynamics for memory, and an explicit latency pathway. This synthesis allows us to capture history-dependent behavior (via σ) in a framework directly aligned with clinical monitoring schedules, a capability absent in prior models.

8. Conclusion

In this paper, we introduced and analyzed a novel discrete fractional-order model of HIV dynamics that incorporates a pathway to cell latency. Our work demonstrates the value of this combined approach, where the fractional order captures the inherent memory of the biological system and the discrete framework aligns with the nature of clinical data collection. Our mathematical analysis rigorously established the model's well-posedness and the stability conditions for both disease-free and endemic states. The derivation of the basic reproduction number (R_0) and the subsequent sensitivity analysis provided critical insights for therapeutic intervention, identifying viral production and infection rates as the most potent targets for controlling the spread of HIV. Numerical simulations successfully reproduced key clinical features of HIV pathogenesis, including the initial viral burst characteristic of the acute phase and the subsequent stabilization to a chronic infection state. We demonstrated that the fractional order σ is a crucial parameter that modulates the speed of these dynamics. Together, these contributions establish a biologically meaningful and mathematically rigorous framework for exploring HIV latency and memory using discrete fractional dynamics, bridging theoretical analysis with clinical modeling relevance.

8.1 *Limitations and future directions*

While this study establishes a novel and rigorous framework, some limitations present opportunities for future research. First, the model is deterministic; incorporating stochasticity would better capture the random fluctuations inherent in biological systems, such as viral mutation and immune recognition. Second, and most critically, the parameters are drawn from the literature to represent a typical infection. A primary direction for future work is to calibrate and validate the model against longitudinal patient data. This would involve using optimization techniques to estimate parameters like the fractional order σ, the latency rate δ, and the infection rate k from individual patient viral load and $CD4^+$ T-cells trajectories. Such calibration is essential to transform the model from a theoretical tool into a personalized predictive framework. Finally, extending the model to include adaptive immune responses (Cytotoxic T Lymphocytes (CTLs)), antibodies, or Antiretroviral Therapy (ART) dynamics would significantly enhance its clinical applicability.

Data availability

All data generated or analyzed during this study are included within this published article.

Acknowledgments

This study is supported via funding from Prince sattam bin Abdulaziz University project number (PSAU/2025/R/1447).

Authors contribution

Conceptualization, F. Gassem, Mohammed Almalahi and Ria Egami; Formal analysis, Mohammed Almalahi and Abdelaziz Elsayed; Methodology, Mohammed Almalahi, Khaled Aldwoah and Ashraf A. Qurtam; Project administration, Mohammed Almalahi and Khaled Aldwoah; Software, Mohammed Almalahi; Supervision, Khaled Aldwoah; Writing-original draft, F. Gassem, Mohammed Almalahi, Ria Egami, Khaled Aldwoah, Abdelaziz Elsayed and Ashraf A. Qurtam; Writing-review & editing, F. Gassem, Mohammed Almalahi, Ria Egami, Khaled Aldwoah, Abdelaziz Elsayed and Ashraf A. Qurtam. All authors have read and agreed to the published version of the manuscript.

Conflict of interest

The authors declare that they have no conflicts of interest.

References

[1] Heath K, Levi J, Hill A. The joint united nations programme on HIV/AIDS 95-95-95 targets: Worldwide clinical and cost benefits of generic manufacture. *Aids*. 2021; 35(2): S197-S203.

[2] Fauci AS, Pantaleo G, Stanley S, Weissman D. Immunopathogenic mechanisms of HIV infection. *Annals of Internal Medicine*. 1996; 124(7): 654-663.

[3] Deeks SG, Lewin SR, Havlir DV. The end of AIDS: HIV infection as a chronic disease. *Lancet*. 2013; 382(9903): 1525-1533.

[4] Perelson AS. Modelling viral and immune system dynamics. *Nature Reviews Immunology*. 2002; 2(1): 28-36.

[5] Whiteside TL. Immune suppression in cancer: Effects on immune cells, mechanisms and future therapeutic intervention. *Seminars in Cancer Biology*. 2006; 16(1): 3-15.

[6] Perelson AS. Modeling the interaction of the immune system with HIV. In: *Mathematical and Statistical Approaches to AIDS Epidemiology*. Springer; 1989. p.350-370.

[7] Tuncer N, Ghods K, Sreejithkumar V, Garbowit A, Zagha M, Martcheva M. Validation of a multi-strain HIV within-host model with AIDS clinical studies. *Mathematics*. 2024; 12(16): 2583.

[8] AlShamrani NH, Halawani RH, Shammakh W, Elaiw AM. Global properties of HIV-1 dynamics models with CTL immune impairment and latent cell-to-cell spread. *Mathematics*. 2023; 11(17): 3743.

[9] Lichae BH, Biazar J, Ayati Z. The fractional differential model of HIV-1 infection of $CD4^+$ T-cells with description of the effect of antiviral drug treatment. *Computational and Mathematical Methods in Medicine*. 2019; 2019(1): 4059549.

[10] Magin RL. Fractional calculus models of complex dynamics in biological tissues. *Computers & Mathematics with Applications*. 2010; 59(5): 1586-1593.

[11] van Eekeren LE, Matzaraki V, Zhang Z, van de Wijer L, Blaauw MJ, de Jonge MI, et al. People with HIV have higher percentages of circulating $CCR5^+$ $CD8^+$ T-cells and lower percentages of $CCR5^+$ regulatory T-cells. *Scientific Reports*. 2022; 12(1): 11425.

[12] Petkov S, Bekele Y, Lakshmikanth T, Hejdeman B, Zazzi M, Brodin P, et al. High CD45 expression of $CD8^+$ and $CD4^+$ T-cells correlates with the size of HIV-1 reservoir in blood. *Scientific Reports*. 2020; 10(1): 20425.

[13] Tarancon-Diez L, Carrasco I, Montes L, Falces-Romero I, Vazquez-Alejo E, Jiménez de Ory S, et al. Torque teno virus: A potential marker of immune reconstitution in youths with vertically acquired HIV. *Scientific Reports*. 2024; 14(1): 24691.

[14] Dayan F, Ahmed N, Bariq A, Akgül A, Jawaz M, Rafiq M, et al. Computational study of a co-infection model of HIV/AIDS and hepatitis C virus models. *Scientific Reports*. 2023; 13(1): 21938.

[15] Raza A, Ahmadian A, Rafiq M, Salahshour S, Naveed M, Ferrara M, et al. Modeling the effect of delay strategy on transmission dynamics of HIV/AIDS disease. *Advances in Difference Equations*. 2020; 2020(1): 663.

[16] Raza A, Rafiq M, Baleanu D, Shoaib Arif M, Naveed M, Ashraf K. Competitive numerical analysis for stochastic HIV/AIDS epidemic model in a two-sex population. *IET Systems Biology*. 2019; 13(6): 305-315.

[17] Diethelm K, Ford NJ. *The Analysis of Fractional Differential Equations*. Berlin: Springer; 2010.
[18] Almalahi MA, Ibrahim AB, Almutairi A, Bazighifan O, Aljaaidi TA, Awrejcewicz J. A qualitative study on second-order nonlinear fractional differential evolution equations with generalized ABC operator. *Symmetry*. 2022; 14(2): 207.
[19] Almalahi MA, Aldwoah K, Shah K, Abdeljawad T. Stability and numerical analysis of a coupled system of piecewise Atangana-Baleanu fractional differential equations with delays. *Qualitative Theory of Dynamical Systems*. 2024; 23(3): 105.
[20] Shutaywi M, Shah Z, Vrinceanu N, Jan R, Deebani W. Exploring the dynamics of HIV and $CD4^+$ T-cells with non-integer derivatives involving nonsingular and nonlocal kernel. *Scientific Reports*. 2024; 14(1): 24506.
[21] Saber H, Almalahi MA, Albala H, Aldwoah K, Alsulami A, Shah K, et al. Investigating a nonlinear fractional evolution control model using W-piecewise hybrid derivatives: An application of a breast cancer model. *Fractal and Fractional*. 2024; 8(12): 735.
[22] Sardar P, Biswas S, Das KP, Gupta V, Khan I, Ismail GM, et al. Qualitative analysis of a novel HIV infection model of macrophage cells in Caputo fractional environment. *International Journal of Biomathematics*. 2025; 2550012: 1-34.
[23] Najafi H, Etemad S, Patanarapeelert N, Asamoah JKK, Rezapour S, Sitthiwirattham T. A study on dynamics of $CD4^+$ T-cells under the effect of HIV-1 infection based on a mathematical fractal-fractional model via the Adams-Bashforth scheme and Newton polynomials. *Mathematics*. 2022; 10(9): 1366.
[24] Yaagoub Z, Sadki M, Allali K. A generalized fractional hepatitis B virus infection model with both cell-to-cell and virus-to-cell transmissions. *Nonlinear Dynamics*. 2024; 112(18): 16559-16585.
[25] Yaagoub Z, Allali K. Fractional HBV infection model with both cell-to-cell and virus-to-cell transmissions and adaptive immunity. *Chaos, Solitons & Fractals*. 2022; 165: 112855.
[26] Aldwoah K, Almalahi MA, Shah K. Theoretical and numerical simulations on the hepatitis B virus model through a piecewise fractional order. *Fractal and Fractional*. 2023; 7(12): 844.
[27] Baleanu D, Jajarmi A, Sajjadi SS, Mozyrska D. A new fractional model and optimal control of a tumor-immune surveillance with non-singular derivative operator. *Chaos: An Interdisciplinary Journal of Nonlinear Science*. 2019; 29(8).
[28] Jeelani MB, Alnahdi AS, Abdo MS, Almalahi MA, Alharthi NH, Shah K. A generalized fractional order model for COV-2 with vaccination effect using real data. *Fractals*. 2023; 31(04): 2340042.
[29] Algolam MS, Almalahi M, Aldwoah K, Awaad AS, Suhail M, Alshammari FA, et al. Theoretical and numerical analysis of the SIR model and its symmetric cases with power caputo fractional derivative. *Fractal and Fractional*. 2025; 9(4): 251.
[30] Aldwoah KA, Almalahi MA, Shah K, Awadalla M, Egami RH. Dynamics analysis of dengue fever model with harmonic mean type under fractal-fractional derivative. *AIMS Mathematics*. 2024; 9(6): 13894-13926.
[31] Abdeljawad T. On Riemann and Caputo fractional differences. *Computers & Mathematics with Applications*. 2011; 62(3): 1602-1611.
[32] Shi Y, Wang Z. Bifurcation analysis and chaos control of a discrete fractional-order Leslie-Gower model with fear factor. *AIMS Mathematics*. 2024; 9: 30298-30319.
[33] He ZY, Abbes A, Jahanshahi H, Alotaibi ND, Wang Y. Fractional-order discrete-time SIR epidemic model with vaccination: Chaos and complexity. *Mathematics*. 2022; 10(2): 165.
[34] Al-Khedhairi A, Elsadany AA, Elsonbaty A. On the dynamics of a discrete fractional-order Cournot-Bertrand competition duopoly game. *Mathematical Problems in Engineering*. 2022; 2022: 8249215.
[35] Aldwoah K, Almalahi MA, Abdulwasaa MA, Shah K, Kawale SV, Awadalla M, et al. Mathematical analysis and numerical simulations of the piecewise dynamics model of Malaria transmission: A case study in Yemen. *AIMS Mathematics*. 2024; 9(2): 4376-4408.
[36] Peng Y, He S, Sun K. Chaos in the discrete memristor-based system with fractional-order difference. *Results in Physics*. 2021; 24: 104106.
[37] Ferreira J, Pena G. FDM/FEM for nonlinear convection-diffusion-reaction equations with Neumann boundary conditions-Convergence analysis for smooth and nonsmooth solutions. *Journal of Computational and Applied Mathematics*. 2024; 446: 115866.

[38] Barzehkar N, Jalilian R, Barati A. Hybrid cubic and hyperbolic b-spline collocation methods for solving fractional Painlevé and Bagley-Torvik equations in the Conformable, Caputo and Caputo-Fabrizio fractional derivatives. *Boundary Value Problems*. 2024; 2024(1): 27.

[39] Bivani S, Ghasemi M, Goligerdian A. Fractional b-spline collocation method for the numerical solution of the fractional pantograph differential equations. *Boundary Value Problems*. 2025; 2025(1): 17.

[40] Yiung YL, Yatim SAM. A review on some numerical methods on solving the fractional initial value problems of fractional differential equations. *IAENG International Journal of Applied Mathematics*. 2025; 55(9): 2776-2787.

[41] Perelson AS, Kirschner DE, de Boer R. Dynamics of HIV infection of $CD4^+$ T-cells. *Mathematical Biosciences*. 1993; 114(1): 81-125.

[42] Perelson AS, Nelson PW. Mathematical analysis of HIV-I dynamics in vivo. *SIAM Review*. 1999; 41: 3.

[43] Jan R, Alsulami M, Razak NNA. Modeling the response of the immune system to HIV-tumor interaction via a fractional framework. *European Journal of Pure and Applied Mathematics*. 2025; 18(1): 5670-5670.

[44] George R, Etemad S, Avcı I, Alshammari FS. A qualitative study for two discrete fractional delta difference BVPs with falling functions: Application on the temperature control system. *Qualitative Theory of Dynamical Systems*. 2025; 24(1): 24.

[45] Castillo-Chavez C, Song B. Dynamical models of tuberculosis and their applications. *Mathematical Biosciences and Engineering: MBE*. 2004; 1: 361-404.

[46] Tverdyi D, Parovik R. Investigation of finite-difference schemes for the numerical solution of a fractional nonlinear equation. *Fractal and Fractional*. 2021; 6(1): 23.